Economic Payback Time of Battery Pack Replacement for Hybrid and Plug-In Hybrid Electric Vehicles

Pier Giuseppe Anselma, *Member, IEEE*, Phillip J. Kollmeyer, *Member, IEEE*, Stefano Feraco, Angelo Bonfitto, Giovanni Belingardi, Ali Emadi, *Fellow, IEEE*, Nicola Amati, and Andrea Tonoli

***Abstract*— This article investigates the economic viability of replacing the high-voltage battery pack of a power-split hybrid electric vehicle (HEV) and a plug-in hybrid electric vehicle (PHEV) by estimating the impact of battery aging on the fuel economy, drivability capability, and electric range. The HEV is modeled first, an optimal energy management strategy based on dynamic programming is then implemented, and experimental characterization data for the battery cell is presented. The batteries are tested to a heavily aged state, with up to an 84% loss of capacity. The battery pack payback period is estimated by assessing the vehicle operative costs in terms of fuel and electricity as obtained through numerical simulations as a function of battery aging. Replacing the battery pack at the conventional end-of-life limit of 80% residual capacity is suggested not to be convenient from an economic standpoint for both the HEV and the PHEV. On the other hand, acceptable payback periods (i.e., 2–5 years) can be achieved for the battery pack when being replaced at 20% to 40% residual capacity. The proposed methodology can be implemented to advise an HEV or PHEV user regarding the benefit of replacing the battery pack due to excessive aging.**

***Index Terms*— Battery aging, battery state-of-health (SOH), drivability, electrified powertrain, fuel economy, hybrid electric vehicle (HEV), optimal control.**

I. Introduction

HYBRID electric vehicles (HEVs) are a promising technology to reduce tailpipe emissions without depending on charging infrastructure like pure electric vehicles [1], [2], [3]. In HEVs, high-voltage batteries play a crucial role providing a second bidirectional energy source in the vehicle. Internal combustion engines (ICEs) in HEVs can operate more efficiently through their synergetic cooperation with the electric motor/generators (EMs) that are powered by batteries [4], [5], [6]. Moreover, vehicle batteries enable storing electrical energy harvested in regenerative braking for future use as propelling energy [7]. It is, therefore, crucial that the battery operates effectively throughout the entire HEV lifetime, even as the battery ages significantly [8], [9].

As batteries age their properties change, internal electrical resistance increases, capacity decreases, and the open-circuit voltage characteristics may change, leading to reduced capability [10], [11]. Aging of high-voltage batteries for electrified vehicles is a growing research topic as electrified vehicles become more prevalent and those in the field reach an advanced stage of life [12], [13]. In particular, a compelling research question arises concerning the convenience of replacing the battery pack over the electrified vehicle lifetime. On the one hand, replacing the battery pack at the conventional end-of-life limit of 80% residual capacity ensures that the electrified vehicle achieves similar performances in terms of fuel and energy economy and drivability capability. On the other hand, even though high-voltage batteries can be reused in a second-life application [14], replacing an HEV battery pack is a costly operation for the user and involves additional CO_2 emissions to produce a new battery pack [15]. Therefore, it becomes crucial to develop numerical tools capable of properly assessing the impact of battery pack aging on the energy economy performance and drivability of electrified vehicles. Such analysis allows providing an estimate to HEV and plug-in hybrid electric vehicle (PHEV) users of how much fuel and electrical energy consumptions increase, the electric range decreases, and acceleration capability decreases as the high-voltage battery progressively ages. Moreover, the payback period for replacing the battery pack of the electrified vehicle can be estimated based on the forecast worsening of fuel and electrical energy economies due to battery aging. The HEV and PHEV user could in turn decide whether to replace the battery pack at the conventional end-of-life limit of 80% residual capacity or to maintain the same battery pack until the loss of capacity and power capability results in unacceptable performance.

Research studies have considered how battery aging impacts several types of vehicles. Herb *et al.* [16] in 2013 modeled the impact of linearly decreasing battery power capability over time on the performance of a fuel cell electric vehicle. In 2015, Saxena *et al.* [17] studied how battery capacity fade and reduced power capability impacts the ability of pure electric vehicles to satisfy daily travel needs. The study, which was based on assumed rather than experimentally measured battery

Manuscript received 19 May 2022; revised 7 August 2022; accepted 20 August 2022. Date of publication 29 August 2022; date of current version 21 February 2023. *(Corresponding author: Pier Giuseppe Anselma.)*

Pier Giuseppe Anselma, Stefano Feraco, Angelo Bonfitto, Giovanni Belingardi, Nicola Amati, and Andrea Tonoli are with the Department of Mechanical and Aerospace Engineering (DIMEAS) and the Center for Automotive Research and Sustainable Mobility (CARS), Politecnico di Torino, 10129 Turin, Italy (e-mail: pier.anselma@polito.it).

Phillip J. Kollmeyer and Ali Emadi are with the McMaster Automotive Resource Center (MARC), McMaster University, Hamilton, ON L8P 0A6, Canada (e-mail: kollmeyp@mcmaster.ca).

Digital Object Identifier 10.1109/TTE.2022.3202792

aging characteristics, suggested that batteries could meet driver needs well after the battery has lost 20%–30% of capacity, which is often considered the threshold for end-of-life. In 2020, Chen *et al.* [18] investigated the effect of adjusting three parameters of an energy management strategy for a series PHEV as the battery aged. Even though the increase in fuel consumption due to battery aging was mitigated through a proper calibration of the energy management parameters, the selected vehicle controller was a reactive rule-based approach which is not guaranteed to achieve the globally minimum fuel consumption control solution [19]. Recently, Tang *et al.* [20] proposed a battery health consumption aware energy management system for an HEV based on deep reinforcement learning; however, the HEV was simulated considering new battery conditions only. While these articles give some insights into the impact of battery aging on vehicle performance, more work utilizing experimentally derived battery aging data is still needed to fully understand how the fuel consumption, electric range, and the acceleration capability of HEVs and PHEVs changes as the battery pack ages. This article aims at advancing in the highlighted research field by providing the following contributions.

1) A numerical framework for assessing the global optimal fuel and electrical energy consumption, electric range, and acceleration capability of HEVs and PHEVs as a function of battery state of health (SOH). Both the reduction of capacity and increase in resistance as the battery ages are considered in the analysis.
2) Application of experimental characterization data for three $LiFePO_4$ cells aged until SOH is as low as 20% to calculate the energy consumption, electric range, and acceleration performance of an HEV and PHEV as a function of battery SOH.
3) Assessment of the economic payback time for replacing the battery pack of both an HEV and a PHEV by comparing the vehicle's fuel and electricity costs with the aged versus the new battery.

Obtained results suggest that replacing the battery pack at the conventional end-of-life limit of 80% SOH is not economically beneficial for either the investigated HEV or PHEV since the payback time is well beyond ten years at this SOH. Once SOH is around 40% or less though, replacement is economically viable for many cases, with payback periods as low as 2–5 years.

This article is organized as follows. The HEV model and the adopted simulation approach are presented first. The experimental results for three $LiFePO_4$ cells are then presented, including residual capacity and power capability at various aging conditions. Results are presented for HEV and PHEV simulations conducted at different levels of battery SOH to assess fuel economy potential, acceleration capability, and PHEV electric range. The convenience of replacing the battery pack is then discussed by assessing the estimated battery pack payback period and the economic cost increase due to vehicle energy economy capability worsening for various levels of battery SOH. Conclusions are finally given.

TABLE I
ASSUMED HEV PARAMETERS

Component	Parameter	Value
Vehicle	Mass	1531 kg
ICE	Capacity	1.8 L
	Power max	72 kW @ 5,000 rpm
	Torque max	142 Nm @ 4,000 rpm
EM1	Power max	42 kW
EM2	Power max	65 kW
Transmission	PG ratio (Ring / Sun)	2.6
	Gear ratio (EM2)	1.26
	Final drive ratio	3.27
	Efficiency (EV mode)	0.95
	Efficiency (HEV mode)	0.85
Auxiliaries	Electrical subsystem power	500 W
Battery (HEV)	Pack capacity (1C discharge)	1.82 kWh
	Pack configuration	120S – 2P
	Cell type	A123 ANR26650M1-B
Battery (PHEV)	Pack capacity (1C discharge)	8.87 kWh
	Pack configuration	130S – 9P
	Cell type	A123 ANR26650M1-B

II. HEV MODEL AND CONTROL STRATEGY

A. Representative HEV

The HEV powertrain architecture investigated in this study is representative of the third-generation Toyota Prius[1] hybrid. A spark-ignition Atkinson ICE and two EMs are used in the HEV. The ICE, EM1, and final drive input shaft are, respectively, linked to the carrier, sun gear, and ring gear of a planetary gear (PG) set, a mechanical device that allows decoupling the speed of the ICE and EM1 from the speed of the vehicle. This HEV powertrain is a well-known layout from the state-of-the-art, and open-source data regarding it is available [21]. The HEV parameters used in this analysis are reported in Table I, while the hybrid powertrain configuration is illustrated in Fig. 1. Two high-voltage battery pack configurations are used in this work, a smaller pack for the HEV and a larger pack for the PHEV. Both packs consist of A123 ANR26650M1-B $LiFePO_4$ cylindrical cells, which were experimentally tested as described in Section III. For the HEV, quantity 240 cells in a 120 series, 2 parallel (120S2P) configuration are assumed, resulting in a total stored energy of 1.8 kWh. This pack has similar properties to the third generation Prius's 1.3-kWh NiMH battery pack although the stored energy is somewhat greater. The PHEV battery pack is assumed to consist of quantity 1170 cells in a 130 series, 9 parallel (130S9P) configuration. This pack has 8.87 kWh of stored energy, slightly higher than the pack for the Prius Prime[1] PHEV [26]. The $LiFePO_4$ cell chemistry has been utilized both in medium-voltage and high-voltage battery packs of commercially available HEVs [22], [23]. Moreover, $LiFePO_4$ is recently becoming a popular chemistry choice thanks to lower material cost [24]. Indeed, the $LiFePO_4$ does not involve cobalt or nickel among the required raw material, and it requires less lithium per kWh of capacity compared with nickel manganese cobalt oxide (NMC) or nickel cobalt

[1]Trademarked.

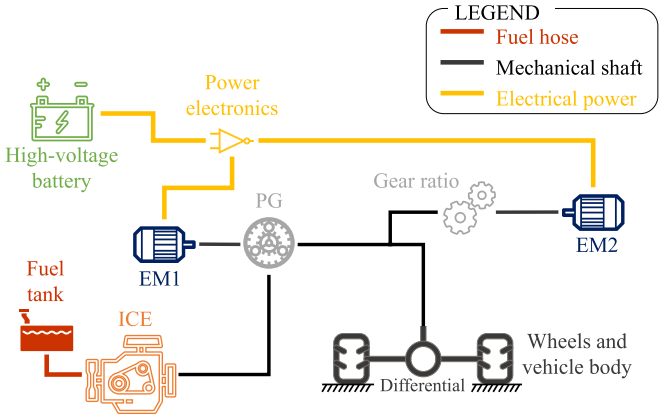

Fig. 1. Toyota Prius hybrid electric powertrain scheme.

aluminum oxide (NCA) chemistries. The much higher energy density of new $LiFePO_4$ cells also makes them much more practical for use in electrified vehicles [25].

B. Modeling Approach

The HEV powertrain operation is modeled using a backward quasi-static approach to derive the requested power values and the speed of components directly from the driving mission requirements (i.e., vehicle speed and acceleration over time) [27]. The value of required torque at the input shaft of the differential T_{FD} is evaluated at each time instant of the driving mission as

$$T_{FD} = \frac{(F_{roll} + F_{misc} + F_{aero} + m_{veh} \cdot \ddot{x}) \cdot r_{dyn}}{\tau_{FD}} \quad (1)$$

where m_{veh}, $\ddot{x}$, r_{dyn}, and τ_{FD} denote the vehicle mass, the vehicle acceleration, the wheel rolling radius, and differential ratio, respectively. F_{aero}, F_{misc}, and F_{roll} are resistive load terms provided by the aerodynamic drag, some various terms (e.g., side forces and road slope), and rolling resistance, respectively.

Looking at Fig. 1, the EM2 angular speed ω_{EM2} is proportionally linked to the angular speed of the differential input shaft ω_{FD}, while the EM1 angular speed ω_{EM1} is a function of the ICE speed ω_{ICE} as well. The resulting kinematic constraints for the HEV drivetrain can then be described as

$$\begin{bmatrix} \omega_{EM1} \\ \omega_{EM2} \end{bmatrix} = \begin{bmatrix} -\tau_{PG} & \tau_{PG}+1 \\ \tau_{GR} & 0 \end{bmatrix} \begin{bmatrix} \omega_{FD} \\ \omega_{ICE} \end{bmatrix} \quad (2)$$

where τ_{PG} denotes the ratio between number of teeth for the ring gear and the number of teeth for the sun gear for the PG, while τ_{GR} is the gear ratio. Considering the torque ratios for standard epicyclic gearing, torque values for both EM1 (T_{EM1}) and EM2 (T_{EM2}) can be evaluated according to the torque request coming from road and driver (T_{FD}) and the torque of the ICE (T_{ICE}), which is implemented as the control variable in the following equation:

$$\begin{bmatrix} T_{EM1} \\ T_{EM2} \end{bmatrix} = \begin{bmatrix} 0 & -\dfrac{1}{\tau_{PG}+1} \\ \dfrac{1}{\tau_{GR} \cdot \eta_{TR}^{\mathrm{sign}(T_{FD})}} & -\dfrac{\frac{\tau_{PG}}{\tau_{PG}+1}}{\tau_{GR}} \end{bmatrix} \begin{bmatrix} T_{FD} \\ T_{ICE} \end{bmatrix} \quad (3)$$

η_{TR} denotes the mechanical efficiency of the transmission, which is powered by the sign of the differential torque in (3) to account for both motoring and braking cases. As reported in Table I, it should be noted that different values of η_{TR} are considered here depending on whether the vehicle is operating in hybrid electric mode or pure electric mode.

The electrical losses of the EMs are modeled by means of empirical lookup tables with speed and torque as independent variables. Then, the electrical power at the battery terminals P_{batt} can be computed by summing the mechanical power values of the two EMs, the electrical losses of the two EMs, and the electrical subsystem power of the auxiliaries (e.g., pumping, lighting, and air conditioning), which is assumed having a constant value in this work.

For the battery, an equivalent circuit model is adopted with open-circuit voltage, internal resistance, charge power capability, discharge power capability, and residual capacity values depending on the instantaneous values of both state of charge (SOC) and SOH [28], [29]. The instantaneous change in battery SOC can, thus, be evaluated as in (4), shown at the bottom of the next page, where R_{IN} and V_{OC} are the internal resistance and the open-circuit voltage of the battery pack. n_P stands for the number of cells in parallel as given by the battery pack configuration, while Ah_{batt} is the battery energy capacity in ampere-hours. The adopted equivalent circuit model considers lumped parameters for the entire battery pack. This involves the assumption that all the series and parallel connected cells of the high-voltage battery pack have the same SOC, SOH, and temperature at each time instant. In the real world, the cells of a battery pack would not have such uniform behavior in terms of SOC, SOH, and temperature among each other. Nevertheless, a detailed model of the individual cells included in the battery pack would remarkably compromise the computational efficiency and the ease of use of the proposed numerical framework. This would in turn impact on the clarity and ease of reading the results presented in this article. The battery temperature is assumed to be a constant value of 25 °C, a value representative of what could be achieved with an effective battery thermal management system. Indeed, modeling the battery temperature variation over time would require both modeling the single cells from a thermal perspective and modeling the thermal management system and its control logic. Also in this case, computational efficiency and ease of understanding the results would be compromised. Moreover, this assumption is in line with the test conditions during the experimental battery tests described in Section III. These two assumptions regarding the high-voltage battery pack constitute necessary limitations for this study, which could, however, be overcome in future work.

C. Fuel Economy Assessment

To estimate the fuel economy of the HEV and of the PHEV in charge sustaining mode, an appropriate energy management strategy needs to be implemented. In this case, the HEV energy management strategy selects at each time instant either pure electric or hybrid operation. If pure electric operation is

selected, only EM2 is activated to either propel the vehicle or to recover electrical energy during regenerative braking. On the other hand, if hybrid mode is enabled, the ICE is in operation and the controller selects the values of ICE speed and ICE torque. In a backward quasi-static approach, knowing speed and torque of the ICE allows automatically determining speed and torque values for the EMs based on the gear ratios. Once speed and torque of the components are known, the instantaneous fuel consumption rate and battery SOC variation can be easily determined. The reader can find details regarding the HEV modeling approach and the related equations in [30].

Dynamic programming (DP) is used here to create a globally optimal HEV control approach. As an off-line method, DP requires the knowledge of the vehicle speed profile for the entire drive cycle before performing the simulation [31], [32]. While DP cannot practically be applied in a vehicle due to its off-line nature and computational cost, DP does provide an upper bound for how well a control policy could perform for this HEV architecture [33], [34]. In this case, DP controls the speed and torque of the ICE and EMs to minimize fuel consumption solely over a predefined drive cycle while sustaining battery charge and limiting the overall number of ICE activations. Particularly, battery charge sustenance is ensured by imposing a constraint on the value of battery SOC at the end of the drive cycle, while the frequency of ICE activations over time is limited by including a dedicated term in the DP cost functional. The optimal HEV control problem to be solved using DP is reported in the following equation, while the related HEV operational constraints are reported in (6)–(16):

$$\arg\min \int_{t_0}^{t_{\text{end}}} [\dot{m}_{\text{fuel}}(t) + \mu_{\text{crank}} \cdot \text{start}_{\text{ICE}}(t)]\, dt \tag{5}$$

s.t. Mechanical constraints:

$$0 \le \omega_{\text{ICE}}(t) \le \omega_{\text{ICE}_{\text{MAX}}} \tag{6}$$

$$\omega_{\text{EM1}_{\text{min}}} \le \omega_{\text{EM1}}(t) \le \omega_{\text{EM1}_{\text{MAX}}} \tag{7}$$

$$0 \le \omega_{\text{EM2}}(t) \le \omega_{\text{EM2}_{\text{MAX}}} \tag{8}$$

$$0 \le T_{\text{ICE}}(t) \le T_{\text{ICE}_{\text{MAX}}}[\omega_{\text{ICE}}(t)] \tag{9}$$

$$T_{\text{EM1}_{\text{min}}}[\omega_{\text{EM1}}(t)] \le T_{\text{EM1}}(t) \le T_{\text{EM1}_{\text{MAX}}}[\omega_{\text{EM1}}(t)] \tag{10}$$

$$T_{\text{EM2}_{\text{min}}}[\omega_{\text{EM2}}(t)] \le T_{\text{EM2}}(t) \le T_{\text{EM2}_{\text{MAX}}}[\omega_{\text{EM2}}(t)] \tag{11}$$

$$\text{ICE}_{\text{ON/OFF}}(t) = [0, 1] \tag{12}$$

Battery constraints:

$$\text{SOC}(t_0) \le \text{SOC}(t_{\text{end}}) \le \text{SOC}(t_0) + \delta \tag{13}$$

$$P_{\text{batt}-\text{min}}(\text{SOC}, \text{SOH}) \le P_{\text{batt}}(t) \le P_{\text{batt}-\text{MAX}}(\text{SOC}, \text{SOH}) \tag{14}$$

$$\text{SOC}_{\text{min}} \le \text{SOC}(t) \le \text{SOC}_{\text{MAX}} \tag{15}$$

$$P_{\text{batt}}(t, \dot{x} < \dot{x}_{\text{lim}}, \ddot{x} < 0) \ge 0. \tag{16}$$

The cost functional to be minimized by DP is reported in (5) and includes $\dot{m}_{\text{fuel}}$ and μ_{crank} denoting the fuel rate consumed by the ICE at each time instant (as computed following the HEV model described) and a constant penalization term for cranking the ICE, respectively. The parameter $\text{start}_{\text{ICE}}$ represents a binary flag detecting ICE cranking events. When solving the optimal HEV control problem, imposed mechanical constraints in (6)–(11) involve limiting torque (denoted as T) and speed (denoted as ω) of the power components within the corresponding allowed operating regions which are specified by the manufacturer of the component. Subscripts "min" and "MAX" refer to the minimum and maximum allowed torques, respectively. Looking at Fig. 1, the EM1 angular speed can have both negative or positive values in (7) depending on the vehicle speed and the controlled ICE speed as shown in (2). On the other hand, the sign of the EM2 angular speed is always positive in (8). For both ICE and EMs, maximum and minimum allowed torque values are retained as a function of the angular speed of the corresponding component in (9)–(11). In (9), the ICE can deliver positive torque only, while in (10) and (11), the torques of the EMs can have negative values as well when generating electrical power. In (12), $\text{ICE}_{\text{ON/OFF}}$ is a binary variable for the ICE state, and values of 0 and 1 relate to the ICE being OFF and ON, respectively. Few constraints are imposed on the battery operation throughout the driving mission in (13)–(16). HEV charge-sustaining operation is achieved by complying with (13), where the battery SOC is set to have similar values at the beginning (i.e., $t = t_0$) and end (i.e., $t = t_{\text{end}}$) of the drive cycle assuming an appropriate tolerance δ. Both battery SOC, battery C-rate, $c(t)$, and battery power, P_{batt}, are constrained within the corresponding allowed operating regions as determined by the battery manufacturer in (14)–(16), respectively. Battery charge and discharge power limits in (14) are calculated based on the SOC and SOH dependent resistance. The charge power is particularly important because it limits how much energy can be captured from regenerative braking. Any energy which cannot be captured is dissipated by friction braking. Finally, in (16), only friction braking is assumed to operate below vehicle speed ($\dot{x}$) values of 10 km/h (denoted as $\dot{x}_{\text{lim}}$), given the limited amount of kinetic energy available to capture at low vehicle speeds [35].

When solving the control problem backwardly from the last time instant of the drive cycle, DP considers the state variables which are the parameters whose evolution throughout the drive cycle depends on the preceding time steps [36], [37]. The states X_{fullHEV} for the HEV powertrain layout are battery SOC and the ICE ON/OFF-state as reported in (2). The control variables U are also listed in the following equation and include ICE speed and torque as discussed at the beginning of this section:

$$X_{\text{HEV}} = \begin{Bmatrix} \text{SOC}(t) \\ \text{ICE}_{\text{ON/OFF}}(t) \end{Bmatrix}; \quad U = \begin{Bmatrix} \omega_{\text{ICE}}(t) \\ T_{\text{ICE}}(t) \end{Bmatrix} \tag{17}$$

where battery SOC is managed to guarantee charge-sustenance and the ICE state (i.e., ON/OFF) is considered to limit the

$$\dot{\text{SOC}} = \frac{V_{\text{OC}}(\text{SOC}, \text{SOH}) - \sqrt{[V_{\text{OC}}(\text{SOC}, \text{SOH})]^2 - 4 \cdot R_{\text{IN}}(\text{SOC}, \text{SOH}) \cdot P_{\text{batt}}}}{2 \cdot R_{\text{IN}}(\text{SOC}, \text{SOH})} \cdot \frac{n_{\text{P}}}{\text{Ah}_{\text{batt}} \cdot 3600} \tag{4}$$

Fig. 2. Experimental setup for tested cells.

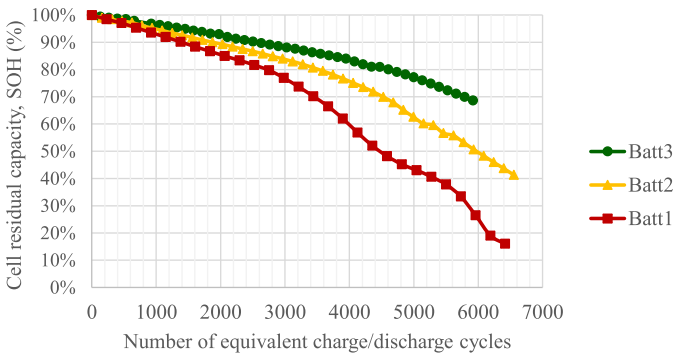

Fig. 3. Trend of residual capacity for the tested cells.

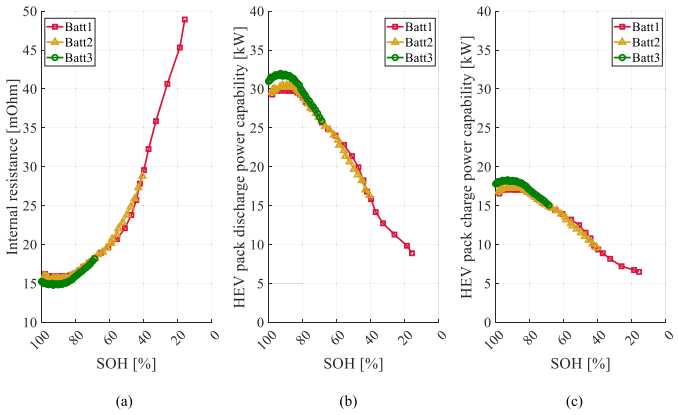

Fig. 4. Experimentally determined cell internal resistance and calculated HEV pack power capability of the tested cells at 50% SOC and as a function of SOH: (a) internal resistance; (b) discharge power capability; and (c) charge power capability.

frequency of cranking events to a reasonable value. The generic "dpm" DP toolbox available in MATLAB[1] is used in this work [38].

D. Acceleration Capability Assessment

In addition to fuel economy, the drivability of the HEV is also evaluated as a function of battery SOH. To this end, acceleration from 0 to 100 km/h is simulated. The time required for the HEV to accelerate from 0–30, 30–60, and 60–100 km/h is then used as an evaluation metric for the performance of the HEV as a function of battery SOH. The same HEV numerical model used for the fuel economy assessment and implemented in MATLAB©software is considered. However, instead of evaluating the HEV powertrain consumption in terms of fuel and battery energy, the maximum amount of tractive power deliverable by the power components is used to simulate the HEV acceleration capability. The time to accelerate to a given speed may increase with aging due to significantly reduced battery power capability, as it will be shown in Section IV-C.

III. Cell Experimental Characterization at Various SOH Values

In a previous work, the authors performed an experimental campaign assessing the aging behavior of three A123 ANR26650M1-B cells subjected to different current profiles associated with an HEV performing the worldwide harmonized light-vehicle test procedure (WLTP) cycle [41]. The current profiles were designed using a numerical aging model to age the battery after approximately 100 thousand, 200 thousand, and 300 thousand km of driving. The three battery cells are referred to in this work as "Batt1," "Batt2," and "Batt3," respectively.

The experimental setup and the trend of the residual capacity over time for the tested cells are shown in Figs. 2 and 3, respectively, while more details regarding the experimental campaign can be found in [41]. Specifically, the cells were placed in an Envirotronics SH16C thermal chamber and temperature was regulated to 25 °C. A ±75-A, 0–5-V rated channel of an MCT 75–0/5-8ME Digatron Power Electronics battery cycler was used to test each cell. Cell voltage was measured at the battery terminals via the battery cycler, and a temperature sensor was fixed to the center of the cylindrical surface of the cell.

The voltage and current measurement and control accuracy of the battery cycler are ±0.1% of full scale, and the accuracy of the temperature sensor is ±0.5 °C. The cycler can regulate voltage from 0 to 5 V, current from −75 to 75 A, and power from −375 to +375 W. The battery cycler utilizes automated software, named "Battery Manager," which is provided by Digatron, Aachen, Germany. It runs on a desktop computer and can be used to create test programs and to save the results in a database. Each program consists of many steps which can be a pause, constant voltage, constant current, or constant power step, or a power or current profile, as is used for the WLTP cycles in this specific case.

Fig. 4(a) shows that internal cell resistance at 50% SOC is relatively constant from 100% until 80% SOH and then steadily increases and doubles by around 40% SOH. Resistance was calculated from a hybrid pulse power characterization (HPPC) test which was repeated periodically throughout the aging tests. Increased resistance results in reduced pack power capability, as is illustrated in Fig. 4(b) and (c), for discharge and charge conditions, respectively, for 50% SOC, an upper battery cell voltage limit of 3.6 V, a lower limit of 2.5 V, and the 240 cell HEV pack. These plots, which were not published in the prior work [41], are used as lookup

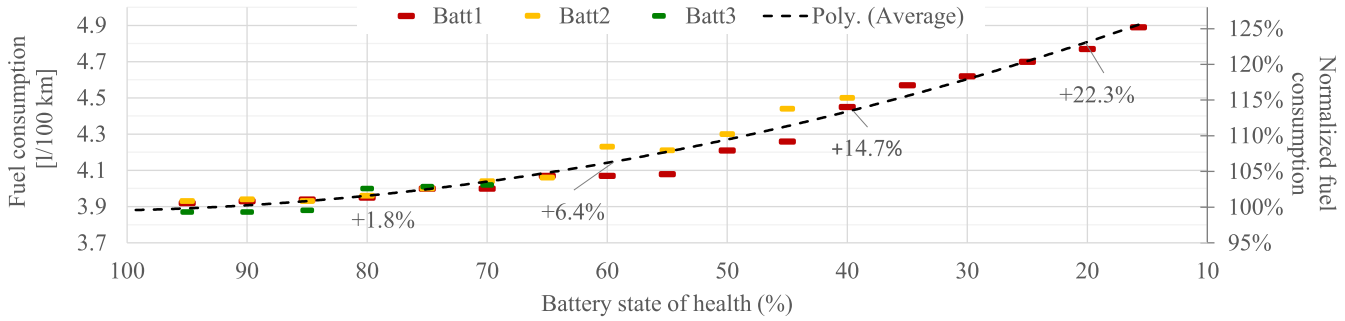

Fig. 5. HEV fuel economy capability predicted by DP in the WLTP over retained battery SOH values for the three test cases and related average.

tables in the HEV model illustrated in Section II. Specifically, the considered battery modeling approach updates the open-circuit voltage and resistance values with respect to the SOC characteristic for each value of the SOH. Then, the charge and discharge power capability is computed at every time step of the simulation, while respecting the voltage limits. An in-depth description of the battery aging modeling approach which is used here can be found in [41], which assumes cell temperature equal to 25 °C.

The analysis uses data for each cell from beginning of life (100% SOH) to the end of the test, 16%, 40%, and 69% SOH for the "Batt1," "Batt2," and "Batt3" test cases, respectively, as reported in Fig. 3.

TABLE II
STATISTICS OF THE HEV OPERATION CONTROLLED BY DP FOR WLTP AND BATTERY SOH VALUES OF 95%, 55%, AND 16% OF "BATT1"

	SOH=95%	SOH=55%	SOH=16%
EM1 loss [kJ]	238	269	422
EM2 loss [kJ]	1063	999	750
Friction brake loss [kJ]	215	560	1645
Battery loss [kJ]	607	581	273
ICE off time [%]	70.9	63.6	27.9
Fuel consumption [g]	670.4	705.5	845.4
ICE mechanical energy [kJ]	10937	11333	12399
Average ICE efficiency [%]	38	38	34

IV. SIMULATION RESULTS AT VARYING BATTERY AGING CONDITIONS

This section illustrates the simulation results obtained for the power-split HEV powertrain at varying battery aging conditions in terms of fuel economy potential and drivability. Battery SOH values from 95% to 16% in 5% steps are considered. The HEV fuel economy capability as predicted by DP simulations for the WLTP drive cycle is first assessed. Then, HEV performance for the WLTP cycle at beginning, middle, and end of life, i.e., 95%, 55%, and 16% SOH, is compared. The acceleration time for full power acceleration maneuvers is then presented. Variations in electric range and fuel consumption in charge-sustaining operation of the PHEV as predicted by DP are then evaluated as a function of battery SOH. In all the results presented here for a given driving mission, DP is implemented as the global optimal control strategy for the HEV and PHEV powertrains. Finally, the economic convenience of replacing the battery pack is assessed for both the HEV and PHEV by estimating the payback period for the replacement operation.

A. Impact of Aging on Fuel Consumption—HEV

The fuel consumption of the HEV obtained by DP for the WLTP cycle is presented as a function of SOH in Fig. 5. Fuel consumption is calculated for each of the three aged batteries (i.e., "Batt1," "Batt2," and "Batt3"). The three sequences of calculated points are nearly superimposed, thus demonstrating that fuel economy is mostly dependent on SOH and not on how the battery was aged in terms of the magnitude of the current profile iterated over time. For the new battery, fuel consumption is estimated by DP to be approximately 3.91 L/100 km for the WLTP drive cycle, which is about 17% less than the 4.7 L/100 km which the model year 2010 Toyota Prius[1] Hybrid is rated for [42]. Considering that the vehicle's rated fuel economy is not calculated on the basis of WLTP drive cycles but from weighted urban dynamometer driving schedule (UDDS) and highway fuel economy test (HWFET) cycles scaled by a correction factor, the model fuel economy matches the rated fuel economy rather well. Several aspects of the modeling may also contribute to the marginal difference, including: 1) the simplified HEV modeling approach, which neglects transient phenomena and some thermal aspects; 2) the lookup tables used for modeling power components, which may include some approximations; 3) the considered cell type (i.e., A123 ANR26650M1-B), which is different than the cells used in the Prius[1]; and 4) the HEV energy management strategy, since DP is different than a real-time control strategy. Still, in the authors' opinion, the above mentioned aspects do not affect the validity of the shown results.

In Fig. 5, fuel consumption is shown to be relatively flat during the first 20% of aging, with fuel consumption increasing by only 1.8% at 80% SOH. Beyond 80% SOH, the battery power capability begins to decrease, as shown in Fig. 4, and as a result, fuel consumption starts to increase significantly, reaching a 10% increase at 50% SOH and a 25.2% increase at 16% SOH. These results suggest that beyond 80% SOH, and especially beyond 50% SOH, there will be noticeable fuel economy benefits when replacing the pack.

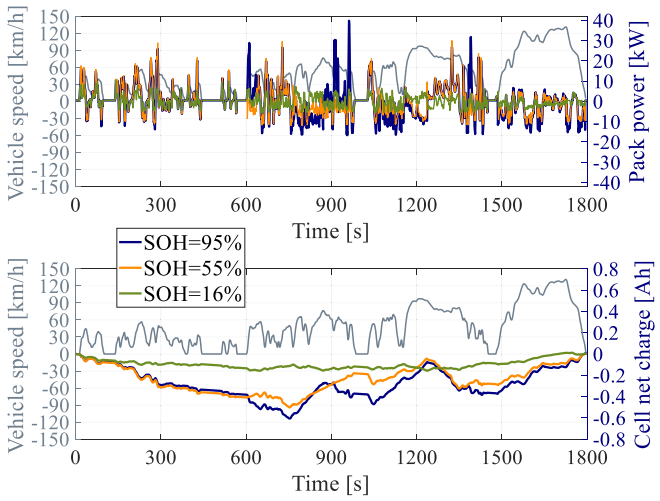

Fig. 6. Battery pack power and SOC as predicted by DP for WLTP and battery SOH values corresponding to 95%, 55%, and 16% of "Batt1."

B. Impact of Battery Aging During WLTP Cycle—HEV

To demonstrate how the HEV powertrain's use of the battery varies with aging, the powertrain performance is simulated using DP for 95%, 55%, and 16% SOH data for Batt1. Fig. 6 illustrates battery pack power and net charge in amp-hours over time for the three aging cases, while Table II reports corresponding loss and performance statistics for the overall drive cycle. The EM and ICE losses are calculated using the corresponding look up tables, the battery loss is determined from the HPPC resistance, and the friction brake loss is all the kinetic braking energy which could not be captured by the electric drive system due to limited battery power capability.

As the cell ages, power capability and capacity are reduced, resulting in a substantial reduction of charge and discharge current and consequently a reduction of net charge used from the battery as shown in Fig. 6. This reduced use of the battery has two primary impacts on vehicle fuel economy. First, the battery is capable of capturing much less regenerative braking energy, resulting in around eight times more friction brake loss when SOH has reduced to 16%, as shown in Table II. Second, the system is not able to shut the ICE OFF as often and operate only at the most efficient points, causing ICE efficiency to reduce from 38% to 34%, as also shown in Table II.

Table II also shows that EM1, which is linked directly with the ICE via the planetary gearbox, has loss increase with battery aging due to increased use of the ICE. EM2 loss decreases by a similar amount though, due to less time spent in electric mode. Even though battery resistance increases with age, battery loss ends up decreasing as the battery ages because loss is a quadratic function and power capability is linear, thus meaning loss falls faster than power capability.

C. Impact of Battery Aging on Drivability—HEV and PHEV

To characterize the drivability of the HEV and the PHEV, a 0–100-km/h full power acceleration was simulated. For both the HEV and PHEV, the time required to complete the maneuver is plotted in Fig. 7 for different levels of battery aging while highlighting the time required to complete three

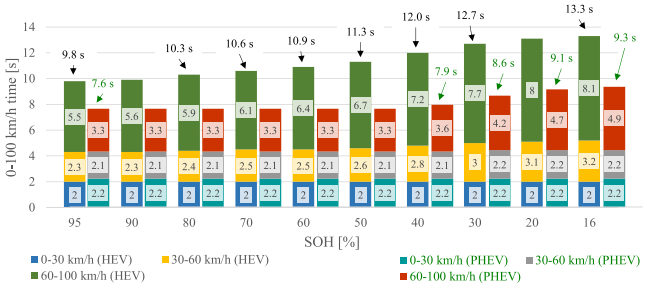

Fig. 7. HEV acceleration performance in 0–30-, 30–60-, and 60–100-km/h full power acceleration maneuvers over retained battery SOH values for both the HEV and PHEV.

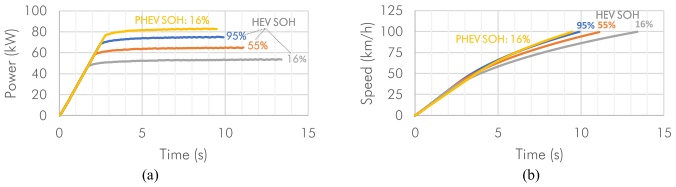

Fig. 8. Time series of drivetrain power and vehicle speed in 0–100-km/h full power acceleration maneuver for battery SOH values corresponding to 95%, 55%, and 16% for the HEV with "Batt1" and 16% for the PHEV with "Batt1": (a) HEV drivetrain power and (b) vehicle speed.

acceleration submaneuvers: 0–30, 30–60, and 60–100 km/h. Battery characteristics at each SOH are assumed to be an average of the three test cases. With a new battery, the full HEV can accelerate from 0 to 100 km/h in 9.8 s, which aligns with the performance of the actual Prius [43], thus further validating the model. The acceleration time of the full HEV increases by 5%, 11%, 22%, and 36% at SOH values of 80%, 60%, 40%, and 16%, respectively. The acceleration rate is relatively stable until 80% SOH and increases substantially with further aging. The 60–100-km/h acceleration time is most affected because the drivetrain is operating in the peak power region here, rather than in the peak torque region as at lower speeds. Peak battery pack power is reduced considerably with aging, as shown in Fig. 4. This in turn affects the maximum tractive power deliverable by the drivetrain of the HEV, as can be seen in Fig. 8 which shows drivetrain power and vehicle speed for 0–100-km/h full power accelerations for different states of aging of Batt1. The drivetrain peak tractive power, which is a function of ICE, EM1, EM2, battery, and transmission power, reduces from 74 kW for new battery conditions to 64 kW for SOH = 55% and down to 53 kW when SOH = 16%. These results demonstrate that power capability reduces steadily with battery aging.

Concerning the PHEV, a new battery pack allows accelerating from 0 to 100 km/h in 7.6 s. Compared with the full HEV, reducing the 0–100 km/h acceleration by 2.2 s is enabled by the increased battery pack power capabilities of the PHEV. The acceleration capability of the PHEV remains stable even for lower battery SOH values (i.e., 50%). This relates to the PHEV acceleration performance not being constrained by the battery pack power capabilities when its SOH ranges from 95% to 50%, but rather by the EM2 torque capability. For heavily aged battery conditions (i.e., SOH = 16%), the 0–100-km/h acceleration time increases to 9.3 s, which is still lower than

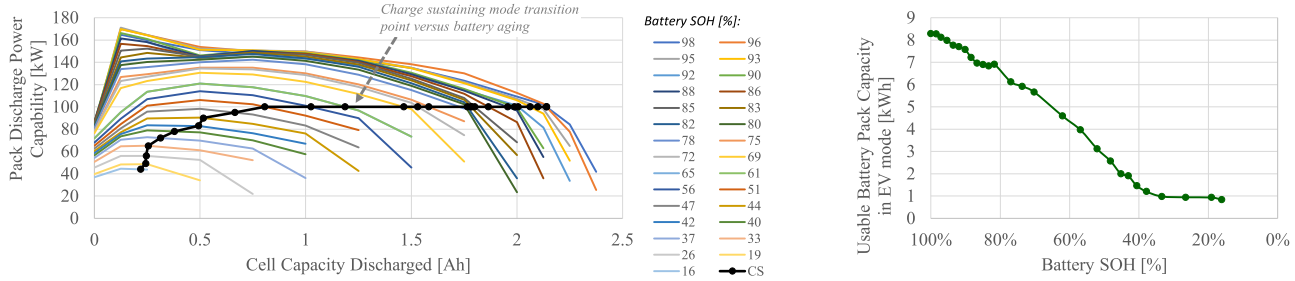

Fig. 9. Discharge power capability and usable capacity in pure electric mode for the PHEV battery pack: (a) PHEV battery pack discharge power capability as a function of battery SOH and (b) usable battery capacity by the PHEV in pure electric mode.

the 0–100 km/h of the HEV with a new battery. These results show that battery aging does not have a significant impact on the acceleration capability of PHEVs.

D. Impact of Aging on Electric Range and Charge-Sustaining Fuel Consumption—PHEV

For the PHEV, both charge-depleting and charge-sustaining modes must be considered when assessing the impact of battery aging. When starting with a full charge, a PHEV typically operates in pure electric, charge depleting mode until much of the usable battery energy has been discharged. Then, the vehicle transitions from charge depleting mode, where the engine is OFF, to charge sustaining mode where the engine may be ON and the vehicle operates like the HEV [44], [45]. In this work, the transition point to charge sustaining mode is defined as the point when battery power capability falls below 100 kW. This value, which has some extra margins, was chosen to ensure that EM2 can deliver its maximum power of 62 kW in both vehicle operating modes. Fig. 9(a) illustrates the PHEV pack discharge power capability, which is calculated from the experimental results, for each tested value of battery SOH. The transition point steadily reduces with decreasing battery SOH, and once battery SOH falls below 50%, it can no longer supply 100 kW so transition points with derated power are instead selected. Fig. 9(b) shows the resulting usable capacity of the PHEV battery pack as a function of its SOH.

The PHEV powertrain performance is then simulated in MATLAB[1] software using DP and almost the same methodology as for the HEV. The one change is that the DP formulation is updated to simulate both charge-depleting and charge-sustaining operating modes for the PHEV. An additional constraint is required to prevent the ICE from activating in charge-depleting mode. This objective is obtained through an additional state variable ($\text{mode}_{\text{CD-CS}}$), resulting in state variables X_{PHEV} as shown in the following equation:

$$X_{\text{PHEV}} = \begin{Bmatrix} \text{SOC}(t) \\ \text{ICE}_{\text{ON/OFF}}(t) \\ \text{mode}_{\text{CD-CS}}(t) \end{Bmatrix} \tag{18}$$

$\text{mode}_{\text{CD-CS}}$ is a binary state variable whose value is 0 at the beginning of the drive cycle to denote charge-depleting PHEV operation. Then, its value is set to 1 once the PHEV battery is depleted to the transition point. This allows DP to discriminate between charge-depleting and charge-sustaining operation when controlling the HEV powertrain. For the simulations, the battery starts fully charged, and then, in charge sustaining mode, the battery SOC is constrained such that the final value of SOC is similar to that at the transition point.

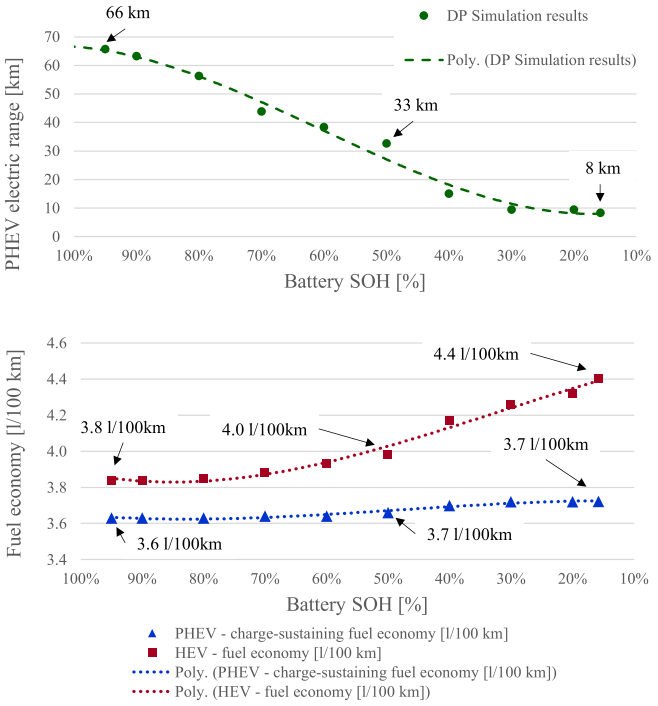

Fig. 10. Electric range and charge-sustaining fuel economy of the PHEV and fuel economy of the HEV as predicted by DP in WLTP over retained battery SOH cases.

Fig. 10 illustrates obtained results in terms of PHEV electric range and fuel economy in charge-sustaining operation in WLTP as a function of battery SOH for both PHEV and HEV. The electric only, charge depleting range is determined by repeating WLTP cycles until the transition point is reached. The simulated range is shown in Fig. 10 to decrease approximately linearly with battery aging, from 66 km for the new pack to just 8 km for the heavily aged pack, which aligns with the usable capacity in Fig. 9(b). The 66-km electric range of the new pack is 26 km greater than the 40-km rated range of the 2017 Toyota Prius[1] Prime [26]. Possible reasons for this mismatch include those listed in Section IV-A

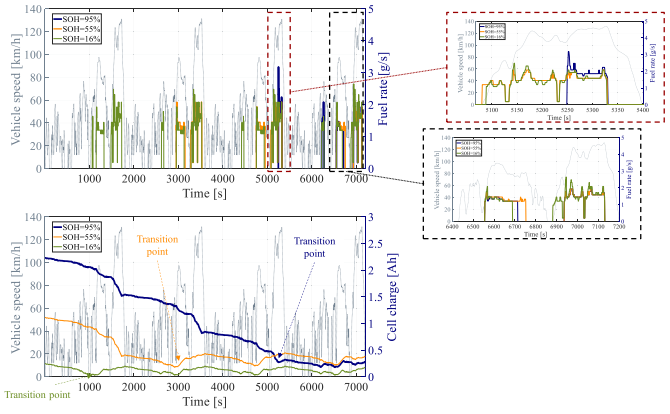

Fig. 11. PHEV fuel rate and cell charge as predicted by DP for four repetitions of WLTP and battery SOH values corresponding to 95%, 55%, and 16%.

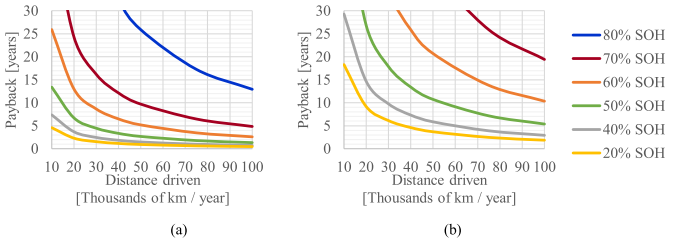

Fig. 12. Battery pack payback period as a function of the battery pack replacement cost, the average yearly distance driven by the HEV user and the SOH of the battery pack at the time of replacement: (a) U.S. $500 pack replacement and (b) U.S. $2000 pack replacement.

as well as that the usable capacity here is around 8.2 kWh while it is closer to 6 kWh for the Prius[1] Prime [46]. The same road load parameters and vehicle mass are also used for the PHEV, but this likely has a minimal impact since the added mass of the battery is similar to the mass of an additional passenger. On the other hand, the trend in predicted fuel economy in charge-sustaining operating mode is quite stable for all the battery SOH cases, oscillating within a small range around 3.7 L/100 km. As the main explanation for the overall constant trend of PHEV fuel economy capability in charge-sustaining mode, Fig. 9(a) highlights how a satisfactory overall battery power capability is preserved even at low values of battery SOH thanks to the increased pack capacity for a PHEV. As consequence, EMs can deliver enough power to allow the ICE operating in highly efficient operating points even at heavily aged battery conditions. The fuel economy of the HEV shown in Fig. 5 is plotted as well in Fig. 10. Looking at this plot, the PHEV is suggested to be further advantageous compared with the HEV from a battery aging perspective since its fuel economy is quite stable with respect to battery SOH. Only 2.6% fuel economy worsening in charge-sustaining operation is observed at 16% SOH compared with new battery conditions, which is a remarkably lower compared with the 25.2% fuel economy increase of the HEV at 16% battery SOH compared with new battery conditions.

Fig. 11 shows the PHEV fuel rate and battery cell charge time-series data as calculated by DP for four repetitions of the WLTP cycle. The results include battery SOH values of 95%, 55%, and 16%. As the battery ages, the transition to charge sustaining operation occurs earlier and earlier, with the transition occurring around 1000 s for the 16% SOH case. Moreover, during charge sustaining operation, DP activates the ICE at higher values of vehicle speed since this minimizes fuel consumption over the drive cycle.

E. Assessing the Economic Convenience of Replacing the Battery Pack—HEV

Estimating the fuel economy capability worsening due to battery aging as performed in Section IV-A opens new possibilities in assessing the economic convenience of replacing the battery pack of the HEV. For the following analysis, few assumptions need to be considered. After being replaced, the performance of the battery pack is assumed not to decay over time. This leads to slightly decrease the estimated pack payback period. Moreover, the HEV user is assumed to accept the worsening in acceleration capability due to battery aging as estimated in Section IV-C. $\mathrm{PB_{HEV}}$, the payback period of a HEV battery pack replacement in years, can then be evaluated as a function of the battery pack replacement cost ($\$_{\mathrm{pack-HEV}}$), the average distance driven by the HEV user in kilometers per year ($\mathrm{km_{year}}$), and the SOH of the battery pack at the time of replacement using the following equation:

$$\mathrm{PB_{HEV}}\left(\$_{\mathrm{pack-HEV}}, \mathrm{km_{year}}, \mathrm{SOH}\right) = \frac{\$_{\mathrm{pack-HEV}}}{\frac{[\mathrm{FE(SOH{=}0.95)-FE(SOH)}]}{100} \cdot \mathrm{km_{year}} \cdot \$_{\mathrm{gasoline}}} \quad (19)$$

where FE is the HEV fuel economy capability in liters per 100 km as a function of the battery SOH. $\$_{\mathrm{gasoline}}$ denotes the gasoline cost, which is retained being U.S. $1.29 per liter here [47].

Fig. 12 illustrates obtained results for the battery pack payback period as a function of $\$_{\mathrm{pack-HEV}}$, $\mathrm{km_{year}}$, and SOH. Particularly, results presented in Section IV-A are considered for extracting the values of FE as a function of SOH. Two cost options are retained for the HEV battery pack replacement being, respectively, U.S. $500 and U.S. $2000. Looking at Fig. 12(a), replacing the HEV battery pack at 80% SOH as standard practice turns out not to be economically convenient. Indeed, the payback period for a U.S. $500 battery pack does not get lower than 13 years even when driving 100 thousand kilometers per year on average. On the other hand, replacing the HEV battery pack progressively gets more economically convenient as the battery SOH gets lower in Fig. 12(a). For example, an HEV user that drives 30 thousands of km per year on average can pay back the new battery pack in 4.5 years (i.e., driving 135 thousands of km) when replacing it at 50% SOH. When the battery SOH gets as low as 20%, the battery pack payback period of 4.5 years can be attained even by a HEV user that drives only 10 thousand of km per year on average. Fig. 12(b) shows that, as the cost for replacing the battery pack gets higher (e.g., U.S. $2000), the economic convenience of such operation considering the operative cost related to fuel consumption gets even lower. For example, an HEV user driving 50 thousands of km per year would need more than ten years to pay back the battery pack replacement when the

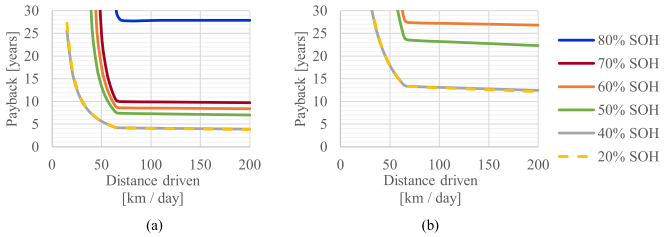

Fig. 13. Battery pack payback period as a function of the battery pack replacement cost, the average daily distance driven by the PHEV user and the SOH of the battery pack at the time of replacement: (a) U.S. $2500 pack replacement and (b) U.S. $8000 pack replacement.

SOH equals 50%. Even for heavily aged battery conditions (i.e., 20% SOH), a 4.5-year payback period can be attained only by driving at least 40 thousands of km yearly. This plots could help an HEV user deciding regarding the convenience of replacing the battery pack.

F. Assessing the Economic Convenience of Replacing the Battery Pack—PHEV

Compared with the HEV, evaluating the economic convenience of replacing the PHEV battery pack involves further calculations. The assumptions performed in Section IV-E hold. Moreover, the battery pack of the PHEV is assumed to be fully charged at the beginning of each day. In this case, the equation for computing the payback period for the PHEV battery pack $\mathrm{PB_{HEV}}$ in years gets more complicated as follows:

$$\mathrm{PB_{PHEV}}\left(\$_{\mathrm{pack-PHEV}}, \mathrm{km_{day}}, \mathrm{SOH}\right) = \frac{\$_{\mathrm{pack-PHEV}}}{\left[\$_{\mathrm{day}}\left(\mathrm{km_{day}}, \mathrm{SOH}\right) - \$_{\mathrm{day}}\left(\mathrm{km_{day}}, \mathrm{SOH}=0.95\right)\right]\cdot 365}. \tag{20}$$

With

$$\begin{aligned}\$_{\mathrm{day}}&\left(\mathrm{km_{day}}, \mathrm{SOH}\right)\\ &= \min\left[\mathrm{km_{day}}; \mathrm{AER(SOH)}\right]\\ &\quad\cdot \$_{\mathrm{electricity}}\cdot\frac{\mathrm{kWh_{AER}(SOH)}}{\mathrm{ER(SOH)}}\\ &\quad+\max\left\{\left[\mathrm{km_{day}}-\mathrm{AER(SOH)}\right];0\right\}\cdot\$_{\mathrm{gasoline}}\cdot\frac{\mathrm{FE(SOH)}}{100}\end{aligned}$$

where $\$_{\mathrm{pack-PHEV}}$ is the cost of the PHEV battery pack replacement, while $\$_{\mathrm{day}}$ is the daily cost associated with the fuel and electricity consumptions of the PHEV as a function of the battery SOH and $\mathrm{km_{day}}$, the average number of kilometers driven by the PHEV user daily. AER and $\mathrm{kWh_{AER}}$ denote the PHEV electric range in kilometers and the usable battery pack capacity in pure electric mode as a function of the battery SOH. Finally, $\$_{\mathrm{electricity}}$ is the electricity cost, which is retained being U.S. $0.16 per kilowatt-hour here [48].

Fig. 13 shows the results obtained for $\mathrm{PB_{PHEV}}$ as a function of $\$_{\mathrm{pack-PHEV}}$, $\mathrm{km_{day}}$, and SOH. Particularly, results presented in Section IV-D are considered for extracting the values of FE, $\mathrm{kWh_{AER}}$, and AER as a function of SOH. Two cost options are retained for the PHEV battery pack replacement being, respectively, U.S. $2500 and U.S. $8000. Both the plots in Fig. 13 feature a knee point corresponding to the AER achievable by the PHEV with a new battery pack (i.e., 66 km). Given the large cost of a PHEV battery pack, the payback period for the PHEV battery pack exponentially increases when the daily driven distance gets lower than 66 km. On the other hand, the payback period exhibits an overall constant trend as the number of daily driven kilometers gets higher than 66 km. This is due to the PHEV fuel economy capability being quite stable at different values of battery SOH as shown in Fig. 10.

Looking at Fig. 13(a), replacing the PHEV battery pack may be suggested only in the case of an intense use of the vehicle. For example, around ten years are required to pay the pack replacement back at 70% SOH. Nevertheless, no advantage is suggested in keeping the same PHEV battery pack when the SOH goes below 40%. Indeed, similar payback periods are observed between 40% SOH and 20% SOH. This relates to similar values of ER being achieved in the range of SOH comprised within 20% and 40%. Moving to Fig. 13(b), all the curves are upshifted compared with Fig. 13(a) due to the higher pack replacement cost. In this case, such high cost generally discourages the PHEV pack replacement. Nevertheless, the similarity between replacing the battery pack at 20% SOH and 40% SOH is preserved. Also, in this case, a PHEV user could use these plots to evaluate the convenience of replacing the PHEV battery pack.

V. Conclusion

HEV batteries continue to function when their capacity has fallen well beyond 80% SOH, the value which is often considered end of life. As battery capacity degrades power capability decreases as well, which impacts the vehicle's performance. Specifically, the reduction in battery power capability prevents the vehicle from accelerating as quickly and recapturing as much regenerative braking energy as when the vehicle was new. The loss of battery capacity and power capability also results in the ICE operating more frequently and at less efficient operating points.

In this study, both a full and a PHEV powertrain layout is investigated using experimentally derived battery characteristics. For the HEV, the degradation of the battery causes a 6% increase in fuel consumption at 60% SOH and a much greater 25% increase at 16% SOH. The 0–100-km/h acceleration time also increases significantly as the battery ages, going from 9.8 s when new to 10.9 s at 60% SOH and to 13.3 s at 16% SOH. For the PHEV, the loss of battery capacity and loss of electric range are correlated, with a 14.4% decrease in electric range at 80% SOH, a 50% decrease at around 50% SOH, and a much greater 87.5% decrease at 16% SOH. On the other hand, predicted charge-sustaining fuel economy of the PHEV remains quite stable thanks to the much higher power capability of the larger PHEV pack, even at low values of SOH.

The economic payback time for replacing the battery pack has been evaluated by calculating how many years it will take for the new battery pack cost to equal the additional fuel and electricity costs that would be incurred if the aged battery was instead continued to be used. For both the HEV and the PHEV, replacing the pack after 20% of capacity loss, which is typically considered end of life, appears to not

be economically beneficial due to excessively long payback periods. For example, for the HEV, with a U.S. $500 battery pack replacement cost, a five year or less payback time can only be achieved once the battery SOH is 40% or less and when driving 18 000 km or more per year. On the other hand, for a higher cost for the pack replacement (i.e., U.S. $2000), the payback period increases to 10–15 years under the same conditions, which discourages the replacement from an economic perspective. As concerns the PHEV, the battery pack replacement is only advisable when the user drives on average more kilometers per day than the pure electric range achievable with a new battery pack. In this case, replacing the battery pack when the SOH is less than 40% is suggested thanks to an acceptable payback time (i.e., less than five years) for a U.S. $2500 pack replacement cost. The payback period would be more than doubled for a higher pack replacement cost (i.e., U.S. $8500), which dissuades swapping the battery pack if the cost is high.

In general, the proposed methodology can be implemented to predict when an HEV or PHEV user is likely to benefit from replacing the battery pack due to excessive aging. When the vehicle user accepts a slight worsening in the vehicle acceleration capability and fuel economy, the use of the battery pack on-board the HEV or PHEV can be extended down to lower values of SOH. In this way, considerable economic savings can be achieved and the CO_2 emissions caused by the manufacturing of new battery packs can be reduced. While this study investigates how the performance degradation of cylindrical lithium iron phosphate (LiFePO4) cells impacts HEVs and PHEVs, the same approach could be applied for battery packs using NMC, NCA Li-ion cells, or nickel metal hydride (NiMH) cells all of which are commonly used in electrified vehicles. The aging properties of these battery types will likely translate to different conclusions regarding the relation between battery aging, increase in fuel consumption, and decrease in electric range for plug-in applications.

Related future work could also aim at overcoming the assumptions introduced in Section II-B by improving the fidelity level of the high-voltage battery pack modeling. Numerical models and control logic related to the difference among the cells in terms of temperature and SOC, along with the pack cooling system, could be implemented to this end. Finally, the HEV simulations performed as the battery ages may be useful for developing more accurate battery state estimation algorithms, robust battery management systems, and HEV energy management strategies capable of adapting to the SOH of the high-voltage battery pack.

ACKNOWLEDGMENT

REFERENCES

[1] B. Bilgin *et al.*, "Making the case for electrified transportation," *IEEE Trans. Transport. Electrific.*, vol. 1, no. 1, pp. 4–17, Jun. 2015.

[2] I. Aghabali, J. Bauman, P. J. Kollmeyer, Y. Wang, B. Bilgin, and A. Emadi, "800-V electric vehicle powertrains: Review and analysis of benefits, challenges, and future trends," *IEEE Trans. Transport. Electrific.*, vol. 7, no. 3, pp. 927–948, Sep. 2021.

[3] X. Hu, J. Han, X. Tang, and X. Lin, "Powertrain design and control in electrified vehicles: A critical review," *IEEE Trans. Transport. Electrific.*, vol. 7, no. 3, pp. 1990–2009, Feb. 2021.

[4] W. Wang, X. Chen, and J. Wang, "Motor/generator applications in electrified vehicle chassis—A survey," *IEEE Trans. Transport. Electrific.*, vol. 5, no. 3, pp. 584–601, Sep. 2019.

[5] N. Leahey and J. Bauman, "A fast plant-controller optimization process for mild hybrid vehicles," *IEEE Trans. Transport. Electrific.*, vol. 5, no. 2, pp. 444–455, Jun. 2019.

[6] W. Lee, E. Schubert, Y. Li, S. Li, D. Bobba, and B. Sarlioglu, "Overview of electric turbocharger and supercharger for downsized internal combustion engines," *IEEE Trans. Transport. Electrific.*, vol. 3, no. 1, pp. 36–47, Mar. 2017.

[7] A. Emadi, "Transportation 2.0: Electrified-enabling cleaner, greener, and more affordable domestic electricity to replace petroleum," *IEEE Power Energy Mag.*, vol. 9, no. 4, pp. 18–29, Jul./Aug. 2011.

[8] L. Tang, G. Rizzoni, and S. Onori, "Energy management strategy for HEVs including battery life optimization," *IEEE Trans. Transport. Electrific.*, vol. 1, no. 3, pp. 211–222, Oct. 2015.

[9] H. Zhu, Z. Song, J. Hou, H. F. Hofmann, and J. Sun, "Simultaneous identification and control using active signal injection for series hybrid electric vehicles based on dynamic programming," *IEEE Trans. Transport. Electrific.*, vol. 6, no. 1, pp. 298–307, Mar. 2020.

[10] R. Xiong, Y. Pan, W. Shen, H. Li, and F. Sun, "Lithium-ion battery aging mechanisms and diagnosis method for automotive applications: Recent advances and perspectives," *Renew. Sustain. Energ. Rev.*, vol. 131, pp. 1–14, Oct. 2020.

[11] *Battery Test Manual for Plug-in Hybrid Electric Vehicles*, U.S. Department of Energy, Idaho National Laboratory, Idaho Falls, ID, USA, Mar. 2008.

[12] N. Shateri, D. J. Auger, A. Fotouhi, and J. Brighton, "An experimental study on prototype Lithium–Sulfur cells for aging analysis and state-of-health estimation," *IEEE Trans. Transport. Electrific.*, vol. 7, no. 3, pp. 1324–1338, Sep. 2021.

[13] X. Hu, Y. Che, and X. Lin, "Battery health prediction using fusion-based feature selection and machine learning," *IEEE Trans. Transport. Electrific.*, vol. 7, pp. 382–398, 2021.

[14] Y. Yang, J. Qiu, C. Zhang, J. Zhao, and G. Wang, "Flexible integrated network planning considering echelon utilization of second life of used electric vehicle batteries," *IEEE Trans. Transport. Electrific.*, vol. 8, no. 1, pp. 263–276, Mar. 2022.

[15] O. Teichert, F. Chang, A. Ongel, and M. Lienkamp, "Joint optimization of vehicle battery pack capacity and charging infrastructure for electrified public bus systems," *IEEE Trans. Transport. Electrific.*, vol. 5, no. 3, pp. 672–682, Sep. 2019.

[16] F. Herb, P. R. Akula, K. Trivedi, L. Jandhyala, A. Narayana, and M. Wohr, "Theoretical analysis of energy management strategies for fuel cell electric vehicle with respect to fuel cell and battery aging," in *Proc. World Electr. Vehicle Symp. Exhib. (EVS27)*, Nov. 2013, pp. 1–9.

[17] S. Saxena, C. Le Floch, J. MacDonald, and S. Moura, "Quantifying EV battery end-of-life through analysis of travel needs with vehicle powertrain models," *J. Power Sources*, vol. 282, pp. 265–276, May 2015.

[18] Z. Chen, J. Lu, B. Liu, N. Zhou, and S. Li, "Optimal energy management of plug-in hybrid electric vehicles concerning the entire lifespan of lithium-ion batteries," *Energies*, vol. 13, no. 10, pp. 2543–2557, 2020.

[19] Z. Pourbafarani, M. Montazeri-Gh, and M. Khasheinejad, "Improvement of PHEV equivalent fuel economy and battery life by applying traffic-based SOC management," *IEEE Trans. Transport. Electrific.*, vol. 8, no. 1, pp. 160–167, Mar. 2022.

[20] X. Tang, J. Zhang, D. Pi, X. Lin, L. M. Grzesiak, and X. Hu, "Battery health-aware and deep reinforcement learning-based energy management for naturalistic data-driven driving scenarios," *IEEE Trans. Transport. Electrific.*, vol. 8, no. 1, pp. 948–964, Mar. 2022.

[21] S. Lee *et al.*, "Modeling and validation of power-split and P2 parallel hybrid electric vehicles," SAE Tech. Paper 2013-01-1470, 2013.

[22] Green Car Congress. *A123 Systems Supplying Li-Ion Batteries for New BMW ActiveHybrid 3 and ActiveHybrid 5 Models*. Accessed: Jul. 19, 2022. [Online]. Available: https://www.greencarcongress.com/2012/01/a123bmw-20120106.html

[23] J. Shepard. *A123 Systems to Supply Lithium Ion Battery Packs to BAE Systems Hybrid Electric Propulsion System*. Accessed: Jul. 19, 2022. [Online]. Available: https://eepower.com/news/a123-systems-to-supply-lithium-ion-battery-packs-to-bae-systems-hybrid-electric-propulsion-system/#

[24] M. Greenfield. *Is LFP Still the Cheaper Battery Chemistry After Record Lithium Price Surge*. Accessed: Jul. 19, 2022. [Online]. Available: https://www.spglobal.com/commodityinsights/en/market-insights/blogs/metals/051122-battery-metals-lithium-cobalt-nickel-prices
[25] S. Kothari. *BYD Blade Battery: Everything You Should Know*. Accessed: Jul. 19, 2022. [Online]. Available: https://topelectricsuv.com/news/byd/byd-blade-battery-update
[26] S. Ichikawa *et al.*, "Development of new plug-in hybrid system for compact-class vehicle," *SAE Int. J. Alternative*, vol. 6, no. 1, pp. 95–102, 2017.
[27] G. Rizzoni, L. Guzzella, and B. M. Baumann, "Unified modeling of hybrid electric vehicle drivetrains," *IEEE/ASME Trans. Mechatron.*, vol. 4, no. 3, pp. 246–257, Sep. 1999.
[28] R. Gu, P. Malysz, H. Yang, and A. Emadi, "On the suitability of electrochemical-based modeling for lithium-ion batteries," *IEEE Trans. Transport. Electrific.*, vol. 2, no. 4, pp. 417–431, Dec. 2016.
[29] A. Bonfitto, S. Feraco, A. Tonoli, N. Amati, and F. Monti, "Estimation accuracy and computational cost analysis of artificial neural networks for state of charge estimation in lithium batteries," *Batteries*, vol. 5, no. 2, pp. 47–63, 2019.
[30] P. G. Anselma, P. Kollmeyer, G. Belingardi, and A. Emadi, "Multi-objective hybrid electric vehicle control for maximizing fuel economy and battery lifetime," in *Proc. IEEE Transp. Electrific. Conf. Expo. (ITEC)*, Jun. 2020, pp. 1–6.
[31] A. Biswas, P. G. Anselma, and A. Emadi, "Real-time optimal energy management of multimode hybrid electric powertrain with online trainable asynchronous advantage actor–critic algorithm," *IEEE Trans. Transport. Electrific.*, vol. 8, no. 2, pp. 2676–2694, Jun. 2022.
[32] H. He, Y. Wang, J. Li, J. Dou, R. Lian, and Y. Li, "An improved energy management strategy for hybrid electric vehicles integrating multistates of vehicle-traffic information," *IEEE Trans. Transport. Electrific.*, vol. 7, no. 3, pp. 1161–1172, Sep. 2021.
[33] B.-H. Nguyen, T. Vo-Duy, M. C. Ta, and J. P. F. Trovao, "Optimal energy management of hybrid storage systems using an alternative approach of Pontryagin's minimum principle," *IEEE Trans. Transport. Electrific.*, vol. 7, no. 4, pp. 2224–2237, Dec. 2021.
[34] W. Zhou, N. Zhang, and H. Zhai, "Enhanced battery power constraint handling in MPC-based HEV energy management: A two-phase dual-model approach," *IEEE Trans. Transport. Electrific.*, vol. 7, no. 3, pp. 1236–1248, Sep. 2021.
[35] S. Heydari, P. Fajri, M. Rasheduzzaman, and R. Sabzehgar, "Maximizing regenerative braking energy recovery of electric vehicles through dynamic low-speed cutoff point detection," *IEEE Trans. Transport. Electrific.*, vol. 5, no. 1, pp. 262–270, Mar. 2019.
[36] P. Elbert, S. Ebbesen, and L. Guzzella, "Implementation of dynamic programming for n-dimensional optimal control problems with final state constraints," *IEEE Trans. Control Syst. Technol.*, vol. 21, no. 3, pp. 924–931, May 2013.
[37] J. Shen and A. Khaligh, "A supervisory energy management control strategy in a battery/ultracapacitor hybrid energy storage system," *IEEE Trans. Transport. Electrific.*, vol. 1, no. 3, pp. 223–231, Oct. 2015.
[38] O. Sundstrom and L. Guzzella, "A generic dynamic programming MATLAB function," in *Proc. IEEE Int. Conf. Control Appl.*, Jul. 2009, pp. 1625–1630.
[39] S. Delprat, T. Hofman, and S. Paganelli, "Hybrid vehicle energy management: Singular optimal control," *IEEE Trans. Veh. Technol.*, vol. 66, no. 11, pp. 9654–9666, Nov. 2017.
[40] O. Sundstrom and L. Guzzella, "A generic dynamic programming MATLAB function," in *Proc. IEEE Int. Conf. Control Appl.*, Jul. 2009, pp. 1625–1630.
[41] P. G. Anselma, P. Kollmeyer, J. Lempert, Z. Zhao, G. Belingardi, and A. Emadi, "Battery state-of-health sensitive energy management of hybrid electric vehicles: Lifetime prediction and ageing experimental validation," *Appl. Energy*, vol. 285, Mar. 2021, Art. no. 116440.
[42] US EPA. *Fuel Economy of the 2010 Toyota Prius*. Accessed: Jul. 19, 2022. [Online]. Available: https://www.fueleconomy.gov/feg/noframes/26425.shtml
[43] *2010 Toyota Prius Performance*. U.S. News & World Report. Accessed: Jul. 19, 2022. [Online]. Available: https://cars.usnews.com/cars-trucks/toyota/prius/2010/performance
[44] S. Zhang and J. Zhang, "Optimal state-of-charge value for charge-sustaining mode of plug-in hybrid electric vehicles," *IEEE Access*, vol. 8, pp. 187959–187964, 2020.
[45] F. Berthold, A. Ravey, B. Blunier, D. Bouquain, S. Williamson, and A. Miraoui, "Design and development of a smart control strategy for plug-in hybrid vehicles including vehicle-to-home functionality," *IEEE Trans. Transport. Electrific.*, vol. 1, no. 2, pp. 168–177, Aug. 2015.
[46] J. O'Dell. *2017 Prius Prime: A Toyota Prius Plug-in You Can Love*. Accessed: Jul. 19, 2022. [Online]. Available: https://thegreencarguy.com/2017-toyota-prius-prime-plug-in-review/
[47] U. S. Energy Information Administration. *Gasoline and Diesel Fuel Update*. Accessed: Jul. 19, 2022. [Online]. Available: https://www.eia.gov/petroleum/gasdiesel/
[48] *Global Petrol Prices*. Accessed: Jul. 19, 2022. [Online]. Available: https://it.globalpetrolprices.com/electricity_prices/

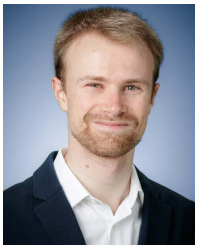

Pier Giuseppe Anselma (Member, IEEE) received the B.S., M.S., and Ph.D. degrees (Hons.) in mechanical engineering from the Politecnico di Torino, Turin, Italy, in 2014, 2017, and 2021, respectively.

In 2016 and 2019, he was a Master's Student Researcher and a Visiting Ph.D. Student Researcher with the McMaster Automotive Resource Centre (MARC), McMaster University, Hamilton, ON, Canada. He is currently a Post-Doctoral Research Fellow with the Politecnico di Torino. He has authored or coauthored more than 60 peer-reviewed international conference and journal publications and holds one patent. His research activities involve the design of propulsion and brake systems and the development of smart and battery sensitive energy management strategies related to electrified and automated road vehicles.

Dr. Anselma has received two awards for his research including the first prize at the TRA Visions 2020 Young Researcher Competition and the Siebel Scholar, class of 2021.

Phillip J. Kollmeyer (Member, IEEE) received the B.S., M.S., and Ph.D. degrees in electrical engineering from the University of Wisconsin–Madison, Madison, WI, USA, in 2006, 2011, and 2015, respectively.

He is currently a Senior Principal Research Engineer with McMaster University, Hamilton, ON, Canada, where his focus is energy storage and electric drivetrain research for transportation applications. He is the Lead Engineer for the 45 member research team working on the Car of the Future Project, which is sponsored by Stellantis NV, Auburn Hills, MI, USA, and Canada's Natural Sciences and Engineering Research Council (NSERC). He has also built a prototype light-duty electric truck, led the development two energy storage research laboratories, and received two awards for his teaching in the electric machines and drives area.

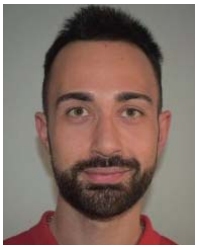

Stefano Feraco received the B.Sc. degree in electrical engineering and the M.Sc. degree in mechatronic engineering from the Politecnico di Torino, Turin, Italy, in 2016 and 2017, respectively, and the Ph.D. degree from the LIM Mechatronics Laboratory, Politecnico di Torino, in 2022.

He is currently an Energy Component Engineer with IVECO Group Company, Turin. His research has been focused on the design and control of autonomous vehicles, virtual sensing, and artificial intelligence for automotive applications.

Angelo Bonfitto received the Ph.D. degree in mechatronics from the Politecnico di Torino, Turin, Italy, in 2010.

He is currently an Assistant Professor with the Department of Mechanical and Aerospace Engineering, Politecnico di Torino. His research is focused on the design and control of active magnetic bearings for rotating machines, active and passive vibration control strategies, and artificial intelligence for automotive applications.

Giovanni Belingardi received the M.S. degree in mechanical engineering from the Politecnico di Torino, Turin, Italy, in 1975.

From 1977 to 1983, he was with the Technical Department, FIAT Auto, Turin. Then, he came back to the Politecnico di Torino and joined the Mechanical Engineering Department, as an Assistant Professor, where he developed his academic carrier up to his present position of Full Professor. He has been appointed as the Director of the Center for Automotive Research and Sustainable Mobility (CARS). He has been and is currently a Scientific Coordinator of the Operative Units, Mechanical and Aerospace Engineering Department, Politecnico di Torino, for a number of projects of the framework programs of the European Union and of the National and Regional Governments. Research cooperation with industrial partners has been effective as well. He is the responsible for International Cooperation of Politecnico di Torino within the frame of the automotive engineering, with particular attention toward Canada, USA, Brazil, Poland, and Serbia. Quite frequent visits of those countries give him a special insight of their situation and needs and allowed him to construct a wide net of partnership. He has authored more than 350 articles published in international scientific journals and in proceedings of national and international conferences.

Ali Emadi (Fellow, IEEE) received the B.S. and M.S. degrees (Hons.) in electrical engineering from the Sharif University of Technology, Tehran, Iran, in 1995 and 1997, respectively, and the Ph.D. degree in electrical engineering from Texas A&M University, College Station, TX, USA, in 2000.

He was the Harris Perlstein Endowed Chair Professor of Engineering and the Director of the Electric Power and Power Electronics Center and Grainger Laboratories, Illinois Institute of Technology, Chicago, IL, USA, where he established research and teaching facilities as well as courses in power electronics, motor drives, and vehicular power systems. He was the Founder, the Chairperson, and the President of Hybrid Electric Vehicle Technologies, Inc. (HEVT), Chicago—a university spin-off company of the Illinois Institute of Technology. He is also the President and the Chief Executive Officer of Enedym Inc., Hamilton, ON, Canada, and Menlolab Inc., Hamilton—two McMaster University spin-off companies. He is currently the Canada Excellence Research Chair Laureate with McMaster University, Hamilton. He is also the holder of the NSERC/FCA Industrial Research Chair in Electrified Powertrains and the Tier I Canada Research Chair in Transportation Electrification and Smart Mobility. He has authored or coauthored over 500 journal articles and conference papers as well as several books, including *Vehicular Electric Power Systems* in 2003, *Energy Efficient Electric Motors* in 2004, *Uninterruptible Power Supplies and Active Filters* in 2004, *Modern Electric, Hybrid Electric, and Fuel Cell Vehicles* (Second Edition) in 2009, and *Integrated Power Electronic Converters and Digital Control* in 2009. He was also an Editor of the *Handbook of Automotive Power Electronics and Motor Drives* in 2005 and *Advanced Electric Drive Vehicles* in 2014 and a Coeditor of *Switched Reluctance Motor Drives* in 2018.

Dr. Emadi was the Inaugural General Chair of the 2012 IEEE Transportation Electrification Conference and Expo (ITEC) and has chaired several IEEE and SAE conferences in the areas of vehicle power and propulsion. He was the Founding Editor-in-Chief of the IEEE TRANSACTIONS ON TRANSPORTATION ELECTRIFICATION from 2014 to 2020.

Nicola Amati received the Ph.D. degree in machine design from the Department of Mechanical Engineering, Politecnico di Torino, Turin, Italy, in 2001.

In 2001, he joined the Politecnico di Torino, as a Faculty Member, where he is currently a Full Professor with the Mechanical and Aerospace Engineering Department. His research interests include analysis, design, and control of electromechanical systems with an emphasis on rotating machinery, active and passive magnetic bearings and dampers, and more-electric systems for automotive applications.

Andrea Tonoli received the Ph.D. degree in machine design from the Politecnico di Torino, Turin, Italy, in 1993.

He joined the Politecnico di Torino, as Faculty Member, in 1994, where he served as the Director of the Mechatronics Laboratory, from 2007 to 2011, and is currently a Full Professor with the Mechanical and Aerospace Engineering Department. His research interests include analysis, design, and control of electromechanical systems with an emphasis on rotating machinery, active and passive magnetic bearings and dampers, piezoelectric transducers for vibration and motion control, and electromechanical systems for automotive applications.

Open Access funding provided by 'Politecnico di Torino' within the CRUI-CARE Agreement